Electromagnetic-field distribution in loaded unstable resonators

M. Lax

Department of Physics of the City College and the Graduate Center of the City University of New York, New York, New York 10031

G. P. Agrawal

AT&T Bell Laboratories, Murray Hill, New Jersey 07974

M. Belic* and B. J. Coffey†

Department of Physics, City College of the City University of New York, New York, New York 10031

W. H. Louisell‡

Department of Physics, University of Southern California, Los Angeles, California 90007

Received May 16, 1984; accepted December 20, 1984

We describe a numerical algorithm for the evaluation of the electromagnetic-field distribution in a loaded unstable resonator. The storage requirements are minimized so that the resulting code can be used for large Fresnel numbers. Edge diffraction is accounted for by a recently developed continuous Fourier-transform algorithm. Use is made of a new gain formula that incorporates the effects of interference between the forward and backward waves. The present method yields improved accuracy over previous methods and enables one to perform calculations for systems with large Fresnel numbers on a medium-sized computer. Numerical results are presented for a loaded confocal unstable resonator to study the effect of the saturated gain on the mode profile. An important conclusion is that the saturated gain does not alter the number of peaks and their relative positions in the intensity distribution. This supports the simplified view that these features arise from edge diffraction and that the saturated gain amplifies each peak by a different amount depending on the peak intensities.

1. INTRODUCTION

In recent years unstable resonators have attracted considerable attention[1–32] both theoretically and experimentally for their use in high-gain lasers. The chief advantage of unstable resonators lies in their offering a large mode volume, adjustable diffraction output coupling, and discrimination against higher-order transverse modes. Since these resonators have high diffraction losses, they are useful whenever the gain per round trip is large and have been used in various high-power laser systems, such as CO_2 and CO gas lasers, Nd:glass lasers, YAG solid-state lasers, and chemical lasers.[3–9]

Unstable resonators have an inherent complication in the theoretical analysis of the electromagnetic field distribution. Since the output is taken across a mirror, diffraction taking place at the sharp mirror edges introduces rapid transverse variation in the optical field. Further, the frequency of the spatial oscillation increases with the resonator Fresnel number F. In the case of an empty unstable resonator, asymptotic methods have been developed to obtain the field distribution for large F.[10,11] The mode structure of the resonator is determined in terms of two parameters, the round-trip magnification M and the Fresnel number F, and appears to be well understood for empty resonators with square as well as circular mirrors.[1,10–17]

An evaluation of the electromagnetic-field distribution in a loaded unstable resonator with a saturated gain medium requires a numerical solution of the nonlinear paraxial-wave equation.[18–32] For the case of rectangular geometry, a mesh of N^2 points, where N is the number of mesh points in a transverse dimension, is chosen to represent the optical field. For a resonator with the Fresnel number F, the value of N should be larger than $2\pi F$ in order to resolve the rapid oscillations of the optical field.[19] Finite-difference schemes are ruled out because of unrealistically large computer-memory and -time requirements. Under certain conditions the thin-sheet gain approximation is found to be adequate[18,33]: Here the continuous gain medium is approximated by a series of thin gain sheets (see Fig. 1) with free propagation between, which is accomplished by a fast-Fourier-transform (FFT) algorithm.[19] Even then the core requirements of the computer code are stringent, and the method has been used in the past for small values of F.[18,19] For large F, the asymptotic approach of Horwitz[10] has been extended to include the gain in a loaded resonator.[24] However, the results are applicable only when gain has a slow spatial variation and is intensity independent.[23,24] Smith[28] has included the effect of gain saturation within the framework of an asymptotic analysis valid for large F. Recently Oughstun[29,31] carried out a numerical analysis of the resonator modes for the active and passive cavities.

In this paper we present the details of a computer code whose modest storage requirements allow it to be run on a medium-sized computer for moderately large values of F. Our nonasymptotic approach is similar to that of Sziklas and Siegman[19] with several significant modifications. The for-

0740-3232/85/050731-12$02.00

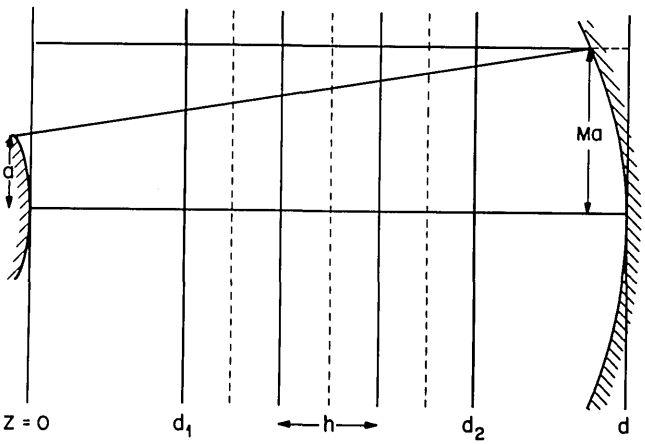

Fig. 1. Illustrating the coordinates and geometry of a positive-branch confocal unstable resonator. A cross-section view of the $y = 0$ plane is shown. Two mirrors at $z = 0$ and $z = d$ are square-shaped spherical mirrors with radii of curvature b_1 and b_2, respectively. The gain medium between planes $z = d_1$ and $z = d_2$ is divided into a number of equispaced segments, and the gain sheets are situated midway on each segment. In the geometrical-optics approximation the light beam expands to a width of Ma, where M is the round-trip magnification. The light that spills over the mirror edges at $z = 0$ is the resonator output.

ward and backward waves are propagated simultaneously,[25] and the gain is calculated whenever needed instead of storing it at various gain sheets. We have developed the continuous-Fourier-transform algorithm to account for edge diffraction.[26,34,35] With the implementation of the CFT and the use of a new modified gain formula,[27] our numerical results are expected to be more accurate than previous calculations.[19]

The plan of the paper is as follows. In Section 2 we obtain the coupled equations for the forward and backward waves, starting from the wave equation, in the paraxial approximation. These equations take into account mutual interference of the forward and backward waves in a standing-wave resonator, an effect important[27] for stationary gain media. The gain medium is modeled by a homogeneously broadened two-level atomic system. Section 3 describes the use of the Fourier-transform technique for solving the nonlinear paraxial-wave equation when the thin-sheet gain approximation is made. The errors associated with the latter approximation are analyzed, and a procedure is described to minimize these errors. The FFT method, although appropriate for the calculations in the gain medium itself, cannot accurately model diffraction at the sharp output mirror edges. We discuss a more accurate approach briefly in Appendix A and refer the reader to recent work[34,35] for details. The boundary conditions appropriate for an unstable resonator are also discussed in Section 3, where the results obtained in the geometrical-optical approximation are described. Section 4 deals with the numerical details of the procedure. By simultaneously integrating the forward and backward waves[25] in the unstable-resonator cavity, we obtain a substantial reduction in memory requirements while slighly hastening convergence. The numerical results obtained for both empty and loaded unstable resonators are presented in Section 5. These results are discussed, and their implications for an actual laser system are mentioned.

2. FIELD EQUATIONS IN THE PARAXIAL APPROXIMATION

We consider an unstable resonator, shown schematically in Fig. 1, with its axis along the z axis, bounded by two square-shaped spherical mirrors at planes $z = 0$ and $z = d$. The gain medium is contained between the planes $z = d_1$ and $z = d_2 > d_1$ and is assumed to be stationary. The electromagnetic field in the resonator is assumed to be monochromatic and linearly polarized (corresponding to a single longitudinal and transverse mode),

$$\mathbf{E}(\mathbf{r}, t) = \mathrm{Re}[\hat{n}E(\mathbf{r})e^{-i\omega t}], \tag{2.1}$$

where $\hat{n}$ is a transverse unit vector and ω is the laser frequency. The complex electric field $E(\mathbf{r})$ satisfies the scalar Helmholtz equation

$$(\nabla^2 + k^2)E(\mathbf{r}) = ikg(|E|^2)E(\mathbf{r}), \tag{2.2}$$

where $k = \sqrt{\kappa_L}\omega/c$ and κ_L is the background linear dielectric constant. The nonlinear saturated gain $g(|E|^2)$ is obtained by modeling the gain medium as a homogeneously broadened two-level atomic system[36] and is given by[37]

$$g(|E|^2) = \frac{g_0(1 + i\Omega)}{1 + \Omega^2 + |E(\mathbf{r})|^2/E_s{}^2}, \tag{2.3}$$

where g_0 is the small-signal on-resonance gain:

$$g_0 = \frac{N_a p^2 D_w \omega}{\sqrt{\kappa_L}\hbar\gamma_{ab}\epsilon_0 c}; \qquad D_w = \frac{\lambda_a}{\gamma_a} - \frac{\lambda_b}{\gamma_b}, \tag{2.4}$$

$E_s = \hbar\gamma_{ab}/p$ is the saturation electric field, and $\Omega = (\omega - \omega_{ab})/\gamma_{ab}$ is the detuning parameter. In Eq. (2.4), N_a is the atomic density, p is the transition atomic-dipole moment, and D_w is the normalized population difference that would be maintained by the pumping mechanism if radiation were inhibited. Here λ_a and λ_b are the pump rates (per atom) into the upper and lower states, respectively; γ_a and γ_b are the corresponding decay rates that are due to spontaneous emission; $\omega_{ab} = \omega_a - \omega_b$ is the atomic frequency difference; and γ_{ab} is the associated homogeneously broadened line width. Further, mks units are adopted, and ϵ_0 is the vacuum permeability. Our algorithm applies, of course, to other nonlinear gain functions as well.

In a standing-wave laser resonator, reflections at the mirrors introduce left-going and right-going waves. The nonlinear denominator in Eq. (2.3) will cause a coupling to all waves of the form $\exp(inkz)$, where n is any odd integer. The most general solution of Eq. (2.2) is assumed to be of the form

$$E(\mathbf{r}) = E_s \sum_{\text{odd } n} \psi_n(\mathbf{r})e^{inkz}, \tag{2.5}$$

where the dimensionless Fourier amplitudes $\psi_n(\mathbf{r})$ are slowly varying functions of $\mathbf{r}$. When Eq. (2.5) is substituted into Eq. (2.2) and Eq. (2.3) is used, one obtains

$$\sum_n e^{inkz}\left[k^2(1 - n^2)\psi_n + 2ink\frac{\partial\psi_n}{\partial z} + \frac{\partial^2\psi_n}{\partial z^2} + \nabla_T^2\psi_n\right]$$
$$= ikg_0(1 + i\Omega)\sum_m \psi_m e^{ikmz}\left(1 + \Omega^2 + \left|\sum_p \psi_p e^{ipkz}\right|^2\right)^{-1}, \tag{2.6}$$

where $\nabla_T^2 = (\partial^2/\partial x^2 + \partial^2/\partial y^2)$ is the transverse part of the Laplacian ∇^2. By taking the appropriate Fourier component

of the right-hand side of Eq. (2.6), one obtains an infinite set of coupled equations for various ψ_n. In the paraxial approximation, $\partial\psi_n/\partial z \ll k\psi_n$, and one neglects $\partial^2\psi_n/\partial z^2$ in Eq. (2.6). Further, for $|n| \neq 1$, the left-hand side of the above equation has a coefficient of order k^2, which makes corresponding ψ_n small. We can obtain an estimate of these terms by neglecting all but the $k^2\psi_n$ term on the left. Thus we find that

$$|\psi_n/\psi_1| \leq (g_0/k), \qquad |n| \neq 1. \tag{2.7}$$

Since the gain per unit wavelength is always quite small ($\approx 10^{-4}$ or less), it is permissible to neglect all terms with $|n| > 1$ and thereby obtain a truncated set of two coupled equations.

In the paraxial approximation, the right-going wave $\psi_R \equiv \psi_1$ and the left-going wave $\psi_L \equiv \psi_{-1}$ satisfy the following equations[27]:

$$\left(2ik\frac{\partial}{\partial z} + \nabla_T^2\right)\psi_R = ikg_R\psi_R, \tag{2.8}$$

$$\left(-2ik\frac{\partial}{\partial z} + \nabla_T^2\right)\psi_L = ikg_L\psi_L, \tag{2.9}$$

$$g_\mu = \frac{g_0(1+i\Omega)}{(a^2-b^2)^{1/2}}\left[1 - \frac{a-(a^2-b^2)^{1/2}}{2|\psi_\mu|^2}\right] \qquad (\mu = R, L), \tag{2.10}$$

$$a = 1 + \Omega^2 + |\psi_R|^2 + |\psi_L|^2, \qquad b = 2|\psi_R||\psi_L|. \tag{2.11}$$

Equation (2.10) represents the modified gain formula. Note that the right- and left-going waves experience different gain because $g_R \neq g_L$. The usual saturation formula[18–22] is obtained when $b = 0$ in Eq. (2.10) and is given by

$$g_R = g_L = \frac{g_0(1+i\Omega)}{1+\Omega^2+|\psi_R|^2+|\psi_L|^2}. \tag{2.12}$$

The gain modification in Eq. (2.10) arises from spatial hole burning resulting from population modulation [in the form of $\exp(2ikz)$] that occurs because of interference between the forward and backward waves. If atoms move because of diffusion, thermal motion, or gas flow, population modulation would be partially washed out. The atoms would have to move more than one-half wavelength during the time the field is reflected back from a mirror for spatial-hole-burning effects to be ignorable. In this case it is more appropriate to use Eq. (2.12). However, for a 10-μm laser with a 3-m cavity length, a speed of 10^3 m/sec would be needed to wash out hole burning. In Section 5 we compare the field distributions obtained using Eq. (2.10) and the conventional choice, Eq. (2.12).

For the special case of a completely symmetric Fabry–Perot resonator with $|\psi_L|^2 = |\psi_R|^2 \equiv I_T/2$ and with $\Omega = 0$, Eq. (2.10) becomes

$$g_R = g_L = \frac{g_0}{I_T}[1 - (1+2I_T)^{-1/2}]. \tag{2.13}$$

Equation (2.13) was first obtained for gain saturation in laser systems with stationary atoms.[38] Recently Eq. (2.10) has also been used to incorporate standing-wave effects in optical bistability,[39–41] where the nonlinear medium inside a Fabry–Perot cavity absorbs the incident radiation. Further, it is possible to integrate analytically Eqs. (2.8) and (2.9) with the gain formula Eq. (2.10) in the plane-wave approximation and with boundary conditions appropriate for a Fabry–Perot resonator.[41,42] This permits one to evaluate the interference effects on laser output and thereby optimize the design parameters to obtain maximum power.

3. SOLUTION TECHNIQUE

A. Thin-Sheet Gain Approximation

Finite-difference schemes for numerical solution of the coupled nonlinear parabolic equations (2.8) and (2.9), although desirable, are not practical because of large core and time requirements. An alternative approach is to approximate the continuous gain medium by a series of equally spaced thin sheets at which the complex gain is assumed to be lumped.[18] This is referred to as the thin-sheet gain approximation.[33] The region between two gain sheets has no gain; here the fields are propagated by using the Fourier-transform method. A FFT algorithm may be used for this purpose, and a substantial saving in time is achieved over finite-difference methods. In this subsection we describe the procedure and analyze errors involved in making the thin-sheet gain approximation. The error analysis was previously performed in the context of beam propagation in the atmosphere.[43,44]

Equation (2.8) can be rewritten as

$$\frac{\partial\psi_R}{\partial z} = [A+B]\psi_R, \tag{3.1}$$

where

$$A = \frac{i}{2k}\nabla_T^2, \qquad B = \frac{1}{2}g_R. \tag{3.2}$$

Let us first consider the special case when B is independent of z. Equation (3.1) can be integrated formally to yield

$$\psi_R(z) = U(z)\psi_R(0), \qquad U(z) = \exp[(A+B)z], \tag{3.3}$$

where dependence on x and y is understood. Note that the operators A and B do not commute. In previous work[19] on loaded unstable resonators the field was first free-propagated between gain sheets and then multiplied by the gain at the sheet. This amounts to the approximation

$$U(z) \approx e^{Az}e^{Bz}. \tag{3.4}$$

An application of the Baker–Hausdorff theorem shows that the errors depend on the commutator $[Az, Bz]$ and are of second order in z. Better accuracy is obtained if, instead of relation (3.4), one uses the relation

$$U(z) = \exp(Az+Bz) = \exp(\tfrac{1}{2}Az)\exp(C)\exp(\tfrac{1}{2}Az), \tag{3.5}$$

where

$$C = Bz - \frac{z^3}{24}[A,[B,A]] - \frac{z^3}{12}[B,[B,A]] + \ldots. \tag{3.6}$$

Thus we see that the single commutators have vanished, and, if the double commutators are neglected, $C \approx Bz$, and the errors are of third order in z. The meaning of Eq. (3.5) is that, in going from 0 to z, the gain sheet should be situated at $z/2$; one should first propagate from 0 to $z/2$ and then apply the overall gain at sheet and propagate from $z/2$ to z. In order to comply with this requirement, it is necessary that all the gain

sheets have an equal separation h from one another. Further, the first and the last sheets should be at a distance $h/2$ from the gain medium boundaries.

The above analysis can readily be extended to incorporate the z dependence of the gain operator $B(z)$. For details we refer to App. B of Ref. 44. The leading error term now depends on the commutator $[A, \partial B/\partial z]$. One uses the prescription

$$\psi_R(z) \approx \exp(\tfrac{1}{2}Az)\exp\left[\int_0^z B(z')dz\right]\exp(\tfrac{1}{2}Az)\psi_R(0). \tag{3.7}$$

The fractional error ϵ in propagating between two gain sheets ($z = h$) is given by

$$\epsilon = \frac{[A, \partial B/\partial z]z^2}{4B} = \frac{h}{8kB}[\nabla_T^2, \Delta B], \tag{3.8}$$

where Eqs. (3.2) have been used and $\Delta B = h(\partial B/\partial z)$ is the change in B over the interval h, the separation of the gain sheets. We use

$$[\nabla_T^2, \Delta B] \approx 2\left[\frac{\partial^2}{\partial x^2}, \Delta B\right] \approx 2\frac{\partial^2}{\partial x^2}\Delta B + 4\frac{\partial}{\partial z}\Delta B\frac{\partial}{\partial x} \approx \frac{6\Delta B}{\delta^2}, \tag{3.9}$$

where δ is a transverse distance over which the gain function B changes. Using Eqs. (3.2), (3.8), and (3.9), we obtain

$$\epsilon \approx \frac{3}{4}\frac{h}{k\delta^2}\frac{\Delta g_R}{g_R} = \frac{3}{4}\left(\frac{h}{d}\right)\left(\frac{a}{\delta}\right)^2\left(\frac{1}{2\pi F}\right)\frac{\Delta g_R}{g_R}, \tag{3.10}$$

where $F = a^2/\lambda d$ is the resonator Fresnel number, a is the output-mirror size, and d is the resonator length. Our criterion given by relation (3.10), is related but not equivalent to the one given by Milonni.[33] As F increases, the fine-grained ripples increase in spatial frequency. Thus (a/δ) increases also, and, for the same accuracy ϵ to be maintained, h must be reduced as F increases, especially when sharp edges are present.

In the thin-sheet gain approximation the integration of Eqs. (2.8) and (2.9) proceeds as follows. The gain medium is divided into M equally spaced segments of length h. The gain sheets are situated midway between these segments (see Fig. 1). Let $\psi_R(z)$ be the field at the beginning of a segment. The field is free-propagated by a distance $h/2$ to arrive at the left-hand side of the gain sheet, where, from formulas (3.2) and (3.7), it is given by

$$\psi_R^{(-)}(z + h/2) = \exp\left[\frac{ih}{4k}\nabla_T^2\right]\psi_R(z). \tag{3.11}$$

At the gain sheet the field $\psi_R^{(0)}$ is multiplied by the integrated complex gain to obtain its value at the other side of the sheet,

$$\psi_R^{(+)}(z + h/2) = \exp\left[\tfrac{1}{2}\int_z^{z+h} g_R(z')dz'\right]\psi_R^{(-)}(z + h/2). \tag{3.12}$$

The field is then free-propagated by $h/2$ to arrive at the beginning of the next segment,

$$\psi_R(z + h) = \exp\left[\frac{ih}{4k}\nabla_R^2\right]\psi_R^{(+)}(z + h/2). \tag{3.13}$$

The three steps indicated by Eqs. (3.11)–(3.13) are repeated M times to complete the propagation in the nonlinear medium. A similar procedure is followed for the left-going wave given by Eq. (2.9).

The integration indicated in Eq. (3.12) is approximated by the trapezoidal rule,

$$\int_z^{z+h} g_R(z')dz' \approx \frac{h}{2}[g_R(z + h) + g_R(z)]. \tag{3.14}$$

However, the saturated gain $g_R(z + h)$ depends on the values of ψ_R and ψ_L at $z + h$ that are not known at the gain sheet at $z + h/2$. It can be calculated, of course, in a self-consistent manner, but the previous calculations make no attempt to do this.[18,19] Instead, the integral in Eq. (3.12) is approximated by the midpoint formula

$$\int_z^{z+h} g_R(z')dz' = hg_R(z + h/2). \tag{3.15}$$

To avoid iterations, a further approximation is made by using $\psi_R^{(-)}$ to compute g_R at the gain sheet.

B. Fourier-Transform Method

Free-space propagation indicated in Eqs. (3.11) and (3.13) is carried out using the Fourier-transform technique.[19] We take the two-dimensional Fourier transform of $\psi_R(y, z)$:

$$\begin{aligned}\tilde{\psi}_R(k_z, k_y, z) &= \mathrm{FT}[\psi_R(x, y, z)] \\ &= \iint \psi_R(x, y, z)\exp[i(k_x x + k_y y)]dxdy.\end{aligned} \tag{3.16}$$

Equation (3.11) is rewritten as

$$\begin{aligned}\psi_R^{(-)}(z + h/2) = (\mathrm{FT})^{-1}\exp\left[-\frac{ih}{4k}(k_x^2 + k_y^2)\right] \\ \times (\mathrm{FT})\psi_R(z),\end{aligned} \tag{3.17}$$

where FT and $(\mathrm{FT})^{-1}$ denote the Fourier-transform and the inverse-Fourier-transform operations, respectively. Under certain conditions these operations can be approximated by discrete Fourier-transform operations. The integrals in Eq. (3.16) are then replaced by a double series:

$$\tilde{\psi}_{mn} \simeq \sum_{k=1}^{N}\sum_{l=1}^{N}\exp\left[\frac{2\pi i(km + ln)}{N}\right]\psi_{kl}. \tag{3.18}$$

If the infinite series can be truncated with reasonable accuracy, using a sufficiently large N, the sum may be performed by using a FFT algorithm.[45,46]

Sziklas and Siegman[19] have derived conditions under which the Fourier integral is well approximated by a finite Fourier series. These conditions were obtained in the context of a diverging beam transformation, which reduces the number of points required to sample the electromagnetic field adequately. Since we have not availed ourselves of the diverging beam transformation, it is instructive to consider how these conditions are modified when the curvature of the mirrors is not transformed away. We consider a uniformly illuminated spherical mirror of half-width a on which the field after reflection is given by

$$\psi(x, 0) = \exp(i\pi Cx^2), \tag{3.19}$$

where $C = -2a^2/\lambda B$, with B the radius of curvature. The field at a distance D in the paraxial approximation is given by

$$\psi(x, D) = (-iF)^{1/2} \int_{-1}^{+1} \exp(i\pi F|x - y|^2)\psi(y, 0)\mathrm{d}y, \tag{3.20}$$

where F is the Fresnel number of the calculation, i.e., $F = a^2/\lambda D$. Outside the geometrical shadow of the beam the integral, Eq. (3.20), may be approximated using the formula

$$\int_a^b \exp[-itf(y)]\mathrm{d}y = \frac{i}{t}\left\{\frac{\exp[-itf(b)]}{f'(b)} - \frac{\exp[-itf(a)]}{f'(a)}\right\}, \tag{3.21}$$

which yields for the intensity at $z = D$

$$|\psi(x, D)|^2 = \frac{F}{4\pi^2}\left[\frac{1}{(F + C - Fx)^2} + \frac{1}{(F + C + Fx)^2} + \frac{2\cos(4\pi Fx)}{(F + C + Fx)(F + C - Fx)}\right]. \tag{3.22}$$

Integrating this expression from G to ∞ and dropping the cosine term for large F, we find that the fraction of energy lost to the region $|x| \geq G$ is given approximately by

$$\epsilon_1(G) \approx \frac{1}{2\pi^2 F}\frac{G}{G^2 - 1 - 2D/B}. \tag{3.23}$$

When the mirror is plane, $B = \infty$ and $G \gg 1$, we find that

$$\epsilon_1(G) \approx \frac{1}{2\pi^2 F}\frac{1}{G - 1}, \tag{3.24}$$

which leads to a condition on the guard-band ratio

$$G \geq 1 + \frac{1}{2\pi^2 F \epsilon_1} \tag{3.25}$$

that is identical to Eq. (16) of Ref. 19. In our simulations for a resonator of length $d = D, D/B = 0.6$, and $G \geq 4$, so that the difference between condition (3.25) and the more complex condition obtained from approximation (3.23) is negligible. However, for higher curvatures, the simpler condition (3.25) may not be sufficiently severe.

In a similar manner we obtain the energy aliased into higher frequencies. The Fourier transform of $\psi(x, 0)$ in Eq. (3.19) is given by

$$\phi(\nu) = \int_{-1}^{+1} \exp(2\pi i\nu x)\exp(i\pi Cx^2)\mathrm{d}x. \tag{3.26}$$

For frequencies $\nu > C$ the phase is stationary outside the interval of integration: We use Eq. (3.21) and find that

$$|\phi(\nu)|^2 = \frac{1}{4\pi^2 C^2}\left[\frac{1}{(1 - \nu/C)^2} + \frac{1}{(1 + \nu/C)^2} + \frac{2\cos(4\pi F\nu)}{(1 - \nu^2/C^2)}\right]. \tag{3.27}$$

The energy aliased into modes with frequencies greater than $\nu_{\max}$ is obtained by integrating this expression from $\nu_{\max}$ to ∞, and the fractional loss is given by

$$\epsilon_2 = \frac{1}{2\pi^2 \nu_{\max}}\frac{1}{1 - (C/\nu_{\max})^2}, \tag{3.28}$$

where the rapidly oscillating term in condition (3.27) has been dropped. For a Fourier transform with N_p points, we have $\nu_{\max} = N_p/4G$. In Eq. (3.26) $C = 2FD/B$, where D is the resonator length and B is the mirror curvature. In order to keep the aliasing error below ϵ_2, therefore, N_p must satisfy

$$N_p \geq \frac{G}{\pi^2 \epsilon_2}[1 + (1 + 16C\pi^2\epsilon_2)^{1/2}]. \tag{3.29}$$

Again, for the case of a plane mirror ($C = 0$), it reduces to the condition given in Ref. 19.

C. Edge Diffraction

In unstable resonators the optical beam emerges from around the edges of a sharp output mirror. The resulting edge diffraction of the reflected wave introduces fine ripples into the electromagnetic-field distribution inside the resonator. As the Fresnel number increases, these rapid transverse oscillations in the field decrease in amplitude but increase in frequency. Accordingly, when the free-space propagation of the reflected edge-diffracted wave is performed using FFT methods, a large number of points is required to obtain even moderate accuracy. Sziklas and Siegman[19] have obtained a condition on N' required to sample the fine-grained ripple at the output mirror that arises from edge diffraction on the opposite edge of the input mirror. They obtain

$$N_p' \geq 4G(G + 1)F = N_p + 8FG, \tag{3.30}$$

where N_p satisfies approximation (3.29) and the second equality follows from condition (3.25) and the choice $\epsilon_1 = \epsilon_2$. This criterion is far more stringent than condition (3.29). As was noted in Ref. 19, it is equivalent to the requirement that the transform be sampled accurately even in regions where the field is small. Lax *et al.*[26] and Lax and Agrawal[34] have proposed an algorithm based on a continuous Fourier transform (CFT) to remedy this deficiency. Recently, Coffey and Lax[35] developed a more efficient CFT algorithm. For completeness the details are presented in Appendix A. In Section 5 we compare the converged resonator field distribution obtained using the FFT with that obtained with the CFT, the distinction arising only at the sharp mirror: Free-space propagation inside the gain medium is effected by using the FFT in both cases.

D. Boundary Conditions

Equations (2.8) and (2.9) describing the propagation of the forward and the backward waves are solved subject to the boundary conditions appropriate for an unstable resonator. The geometry of the resonator is shown in Fig. 1. The output mirror at $z = 0$ and the large mirror at $z = d$ have radii of curvature b_1 and b_2, respectively; R_1 and R_2 are the corresponding intensity-reflection coefficients. When the light beam reflects from any of the two mirrors, the finite curvature of the mirror introduces a space-dependent phase shift. Assuming that the radii of curvature b_1 and b_2 are large in comparison with the beam width, the boundary conditions at the left-hand mirror at $z = 0$ become

$$\Psi_R(x, y, 0) = -\sqrt{R}\Psi_L(x, y, 0)\exp[-ik(x^2 + y^2)/b_1] \tag{3.31}$$

for $|x|, |y| \leq a$ and zero otherwise. R is the mirror reflectivity, and the finite size of the output mirror has been taken into account. The field $\Psi_L(x, y, 0)$ for $|x|, |y| \geq a$ is the laser output and does not get reflected into the resonator. The boundary condition at the right-hand mirror at $z = d$ is

$$\Psi_L(x, y, d) = -\sqrt{R}\Psi_R(x, y, d) \times \exp(2ikd)\exp[-ik(x^2 + y^2)/b_2], \tag{3.32}$$

where the mirror is assumed to be large in comparison with

the beam dimensions. It will be assumed that the laser frequency ω is tuned to the cavity and that

$$kd = m\pi. \tag{3.33}$$

E. Geometrical-Optics Approximation

A qualitative understanding of the resonator behavior can be obtained in the geometrical-optics approximation.[1] In this approximation the diffraction is neglected, and only the geometrical losses arising from beam spreading are incorporated. A useful parameter in such an analysis is the round-trip magnification

$$M = M_R M_L, \tag{3.34}$$

where M_R and M_L are the linear magnifications of the right- and left-going waves, respectively. Applying the imaging formulas of geometrical optics to the resonator configuration of Fig. 1, one obtains

$$M_R = g_1[1 + (1 - 1/g_1g_2)^{1/2}], \tag{3.35}$$

$$M_L = g_2[1 + (1 - 1/g_1g_2)^{1/2}], \tag{3.36}$$

where

$$g_i = \left[1 - \frac{d}{b_i}\right], \qquad i = 1, 2, \tag{3.37}$$

and is not to be confused with the gain g_R and g_L introduced in Section 2. For a positive-branch confocal unstable resonator[1] (see Fig. 1), often employed in actual experimental setups, $b_1 < 0$ and $b_2 > 0$, and $b_1 + b_2 = 2d$. Using Eqs. (3.34)–(3.37), it is easy to verify that $M_L = 1$ and $M = M_R = |b_2/b_1|$.

The empty-resonator modes are characterized by the round-trip magnification M and the Fresnel number (defined with respect to the small mirror)

$$F = a^2/\lambda d = ka^2/(2\pi d), \tag{3.38}$$

where a is the half-width of the small (output) mirror and λ is the radiation wavelength. The equivalent Fresnel number F_{eq} and the collimated, or tube, Fresnel number F_T are given by

$$F_{eq} = \tfrac{1}{2}(M - 1)F, \qquad F_T = M^2F. \tag{3.39}$$

In the geometrical-optics approximation the field equations (2.8) and (2.9) are written in terms of the intensity and the phase variables using $\psi_\mu = \sqrt{I_\mu}\exp(iS_\mu)(\mu = R, L)$; all transverse variation in I_μ and S_μ is neglected. The ray slopes related to $\nabla_T S_\mu$ are found to be independent of z, and their values depend on the magnifications M_R and M_L. Using Eqs. (2.8) and (2.9), the intensities I_R and I_L are found[27] to satisfy the following set of two coupled first-order nonlinear differential equations:

$$\frac{dI_R}{dz} + 2\left[\frac{(M_R - 1)}{d + (M_R - 1)z}\right]I_R = \mathrm{Re}(g_R)I_R, \tag{3.40}$$

$$\frac{dI_L}{dz} + 2\left[\frac{(M_L - 1)}{d + (M_L - 1)(d - z)}\right]I_L = -\mathrm{Re}(g_L)I_L, \tag{3.41}$$

where the factor of 2 in the second term of Eqs. (3.40) and (3.41) is absent for a two-dimensional strip unstable resonator. For the case of an empty resonator, $g_R = g_L = 0$, Eqs. (3.40) and (3.41) are readily solved. In a round trip the intensity decreases by a factor of M^{-2} (M^{-1} for a strip resonator), and the geometrical power loss per round trip that is due to beam spreading is $(1 - M^{-2})$. Note that it is independent of the Fresnel number F given by Eq. (3.38). The power loss obtained by a numerical solution of Eqs. (2.8) and (2.9) is found to be less than the geometrically predicted loss and shows an intricate dependence on F.[1]

To illustrate the effects of mutual gain interference on I_R and I_L, Eqs. (3.40) and (3.41) were solved numerically.[27] It was found that even in the geometrical-optics approximation the interference of the right- and left-going waves modifies the output intensity by more than 10%.

In Section 5 the effects of gain interference on the output intensity and on the transverse variation of the cavity fields are studied in detail. The geometrical-optics solutions presented here serve as a guide and provide a qualitative comparison with the numerical results. We have also used the solution to Eqs. (3.40) and (3.41) to provide starting fields for the full three-dimensional simulation. This approach can enhance the convergence of the iteration procedure and save computer time.

4. NUMERICAL PROCEDURE

In this section we describe the procedure for the numerical solution of Eqs. (2.8) and (2.9) based on the methods of Section 3. Our aim is to develop a computer code with minimum core requirements applicable to resonators of large Fresnel number F.

The calculational procedure adopted in the past[18,19] solves one of the two equations for each half round trip. Equation (2.8) or (2.9) is used when the beam is propagating to the right or to the left, respectively. The calculation of the saturated gain, Eq. (2.10), requires the knowledge of $|\Psi_R|^2$ and $|\Psi_L|^2$ simultaneously. To this end, the intensity $|\Psi_L|^2$ ($|\Psi_R|^2$) is saved in core at the gain sheets when the field Ψ_R (Ψ_L) is being propagated. The core requirements for such a procedure are large and increase with the number of gain sheets. The method was used for small values $F \approx 1$.

It has been pointed out[25] that a substantial reduction in memory is achieved when Eqs. (2.8) and (2.9) are integrated simultaneously. Further, the storage requirements are independent of the number of gain sheets, which is chosen to satisfy the criterion given by expression (3.10). The numerical code that we have developed solves the forward and the backward waves simultaneously and can be used for large values of F.

On the backward propagation of the left- or right-going wave, the corresponding optical field experiences loss instead of gain, and, in unstable resonators, it contracts instead of expanding. The inverse diffraction problem is similar in difficulty to the diffusion equation solved backward in time, and it is expected that the method will have several limitations. This difficulty would be severe if the backward integration were pursued for more than one trip between mirrors. At each mirror, however, the result of the forward integration is used as the starting field for the next backward integration. Thus errors in the backward integration do not accumulate for more than one half-cycle. As long as the distance between the mirrors is less than a diffraction length, there is no difficulty in handling the sharpening, or "undiffraction," that occurs during the backward integration. This criterion is well

satisfied in the case of unstable resonators, since the ratio of the cavity length to the diffraction length $d/l \approx (2\pi F)^{-1}$ and the Fresnel number $F > 1$. The numerical results of Section 5 are obtained using this proposed scheme of simultaneous forward and backward integration of the cavity fields. To compare this scheme with the conventional method,[18,19] in which only the left- or right-going wave is integrated in forward direction and the integrated gain is saved at each gain sheet, we repeated the calculations of the resonator field, and the results of two methods were identical in accuracy. Our method converged more rapidly because, in computing the gain, the most recent values of the intensities are used. The chief advantage of our method, however, is that the memory requirements are reduced by a factor equal to the number of the gain sheets since the need to save the gain at each sheet is obviated.

A transverse mesh of N_xN_y points, where N_x and N_y are a number of points in the x and y directions, respectively, is chosen to represent the complex fields Ψ_R and Ψ_L. In the absence of any transverse flow and inhomogeneities in the gain medium, the mesh is chosen to cover only one quadrant of the x–y plane ($x > 0$ and $y > 0$) after assuming the rectangular symmetry; this reduces the storage by a factor of 4. For square-shaped mirrors, $N_x = N_y$. However, by choosing $N_y = 1$, one obtains results for a strip (one transverse dimension) resonator. A guard-band ratio $G > M$ is chosen to ensure proper working of the FFT (see Ref. 19). Here M is the round-trip magnification given by Eq. (3.34). The mesh dimensions are Ga, where a is the mirror half-width. Other parameters, such as the resonator length d, the mirror curvatures b_1 and b_2, the mirror reflectivity R, the Fresnel number F, the small-signal gain g_0, and the detuning parameter Ω, are supplied to the program.

A known field distribution $\Psi_L(0)$ is chosen to start the iterative procedure. The reflection at the output mirror yields $\Psi_R(0)$ given by Eq. (3.31). To come to the beginning of the gain medium at $z = d_1$ (see Fig. 1), the CFT is used to free-propagate the field $\Psi_R(0)$ to obtain $\Psi_R(d_1)$. Since $\Psi_L(0)$ has no discontinuities, we always use the FFT to propagate the left-going wave *backward* to obtain $\Psi_L(d_1)$ of the previous round trip.

As we mentioned in Section 3, the gain medium is divided into gain sheets whose number is given as input data and is chosen to satisfy the criterion given by expression (3.10). The position of the gain sheets is shown in Fig. 1. The fields Ψ_R and Ψ_L are propagated from one segment to the next following the prescription of Eqs. (3.11)–(3.13) until one obtains the fields $\Psi_R(d_2)$ and $\Psi_L(d_2)$ at the end of gain medium. The integral in Eq. (3.12) for the total integrated gain is approximated by two methods: the trapezoidal rule as in expression (3.14) and the midpoint formula as in Eq. (3.15). When expression (3.14) is used, the integrated gain is obtained *only through a self-consistent iterative procedure*, which requires that Ψ_R and Ψ_L at two adjacent segments be available. The iteration procedure, however, requires four N_xN_y additional locations in memory. Use of Eq. (3.15) makes the code faster and demands less storage capacity. The desired accuracy can often be obtained by increasing the number of gain sheets.

At $z = d_2$, $\Psi_R(d_2)$ is propagated to the mirror at $z = d$, where, on reflection, $\Psi_L(d)$ is obtained. [Thus it is unnecessary to propagate $\Psi_L(d_2)$ to this mirror.] $\Psi_L(d)$ is used for the half round trip from $z = d$ to $z = 0$ to obtain $\Psi_L(0)$, while Ψ_R is propagated backward whenever saturation gain is to be computed in the manner just described. On arrival of the field at $z = 0$ a single round trip has been completed, and the procedure is iterated to convergence. As a crude check on convergence, we compute two quantities, the integrated intensity, proportional to the power P, and the variance $\sigma_x{}^2$ of the intensity distribution at the output mirror at $z = 0$:

$$P = \int |\Psi_L|^2 dx dy, \tag{4.1}$$

$$\sigma_x{}^2 = \frac{1}{P}\int |\Psi_L|^2 x^2 dx dy. \tag{4.2}$$

We assume that convergence has been achieved when the change in both P and σ_x on two successive round trips is less than ϵ, where $10^{-3} \le \epsilon \le 10^{-2}$. A detailed comparison between fields is, however, needed to verify genuine convergence. For empty resonators the fields are renormalized after each round trip, and the iteration is continued until the change in the power loss, $1 - P(\text{current})/P(\text{previous})$, is less than ϵ. For empty-resonator simulations, a simple Gaussian distribution with a prescribed power and variance [given by Eqs. (4.1) and (4.2), respectively] was used as an initial guess for the starting field, $\Psi_L(0)$. For loaded resonator simulations we used the solution to the one-dimensional geometrical-optics equation (3.37) and (3.38) to obtain an estimate of the power levels. This procedure does not, of course, determine the shape of the starting field, and we used either a Gaussian or a rectangular distribution. With the use of the geometrical-optics solution the convergence rates were slightly enhanced compared with the case when the starting power is chosen arbitrarily.

Finally, we note that the gain medium used here has been characterized only by Eq. (2.10): No gain profile has been specified. This omission could lead to numerical instability if the larger relative errors in the fields near $x = G$ were significantly amplified. Therefore a Fermi-function gain profile was used to suppress amplification of the fluctuations in the wings. For numerical purposes, the small signal gain g_0 is replaced by $g_0(x)g_0(y)$, with

$$g_0(x) = \{1 + \exp[20(x_0 - x)]\}^{-1}, \tag{4.3}$$

where $x_0 = 0.8Ga$, G being the guard-band ratio as before. In Section 5 we compare results obtained with and without gain cut.

5. RESULTS AND DISCUSSION

In this section we present the numerical results obtained using the unstable-resonator algorithm described in previous sections. The geometry of the confocal unstable resonator used is shown in Fig. 1. The resonator parameters were chosen corresponding to an actual experimental setup. The mirrors were separated by a distance of 7.3 m, and the 2-m-long gain medium was situated at a distance of 3.3 m from the output mirror at $z = 0$. The small and large mirrors have the radii of curvature, respectively, $b_1 = 11.68$ m and $b_2 = 26.28$ m, and in the confocal geometry used $b_2 - b_1 = 2d$. Further, the left- and right-going wave magnifications are $M_L = 1$ and $M_R = |b_2/b_1| = 2.25$, giving the round-trip magnification $M = M_R \times M_L = 2.25$. The value of M is kept fixed in all the numerical results presented here. The half-width of the large mirror is assumed to be sufficiently greater than Ma, so edge effects from this mirror are negligible. Here a is the small-mirror

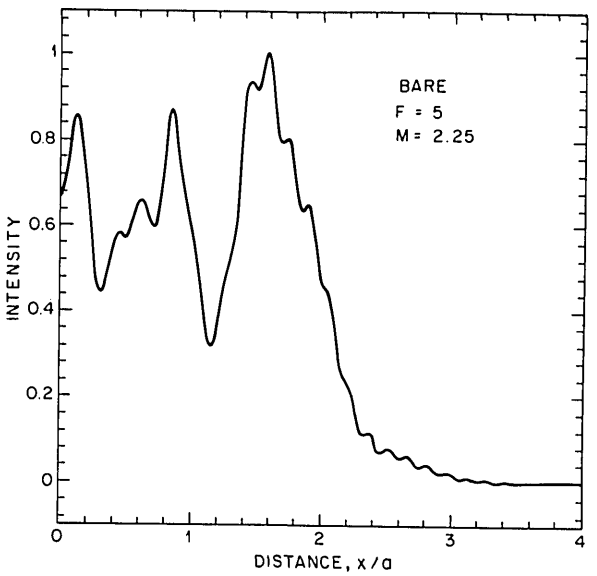

Fig. 2. Normalized intensity distribution at $z = 0$ of the lowest-loss mode of a strip bare confocal unstable resonator with the Fresnel number $F = 5$ and round-trip magnification $M = 2.25$.

half-width. The transverse coordinates x and y are measured in units of a, which therefore enters only through the magnitude of the Fresnel number F given by Eq. (3.38). The guard-band ratio $G = x_{max}/a$ (where x_{max} is the maximum transverse distance at which the field is calculated) is chosen according to the criteria discussed in Section 3. Clearly $G > M$, and we require that the resonator field remain zero for $x \geq Ga$ during the entire simulation. The number of mesh points is chosen according to the criteria specified in Section 3.

A. Bare Resonator

Before presenting our numerical results for a loaded unstable resonator, we briefly consider the case of a strip bare resonator. This is useful for the purpose of code checking. In contrast to previous work, we employ the CFT algorithm that is capable of handling edge diffraction accurately. In Figs. 2 and 3 we show the normalized intensity distribution $|\psi_L(x, 0)|^2$ at the small mirror when the left-propagating wave has just arrived at the plane $z = 0$. The mode profile corresponds to the lowest-loss transverse mode of the unstable resonator. Only the positive half ($x > 0$) region is shown, because of reflection symmetry (about $x = 0$) in the transverse direction. The figures are drawn for a moderate value $F = 5(F_{eq} = 2.8125)$ and for a relatively large value $F = 50(F_{eq} = 28.125)$ of the Fresnel number given by Eq. (3.38). In the geometrical-optics limit $F \to \infty$, the intensity distribution is constant for $|x| < Ma$ and zero outside this region. For finite values of F the detailed qualitative features of the mode profile arise from edge diffraction that introduces spatial oscillations (ripples) in the intensity distribution. A comparison of Figs. 2 and 3 shows that as F increases, the spatial frequency of the ripples increases, while their amplitude decreases as $F^{-1/2}$.[12] Figure 3(b) shows an enlarged view of the intensity profile for $F = 50$ over the region $|x| \leq a$. The phase profiles (not shown) display qualitatively similar behavior. For $|x| \leq Ma$, the phase is almost constant, in accordance with the geometrical-optics approximations. Edge diffraction introduces small deviations whose amplitude decreases with F. Note that the often-used tube Fresnel number $F_T = M^2F$ is about 250 in Fig. 3—much larger than used in most previous work.

To quantify the improvement achieved with CFT, Figs. 4 and 5 show the intensity and the phase profiles of the bare-resonator mode obtained using the CFT and the FFT algorithms. It is important to stress that the two algorithms differ in their performance only when the field has a sharp discontinuity such as the one occurring at the output-mirror edge. Once the field has been propagated away from the output mirror, only the FFT is used in both cases in view of its faster execution. Figures 4 and 5 are drawn for a moderately large value of $F = 10$ with the number of mesh points $N = 200$. A direct comparison shows that significant quantitative deviations (~10%) occur when the FFT is replaced with the CFT.

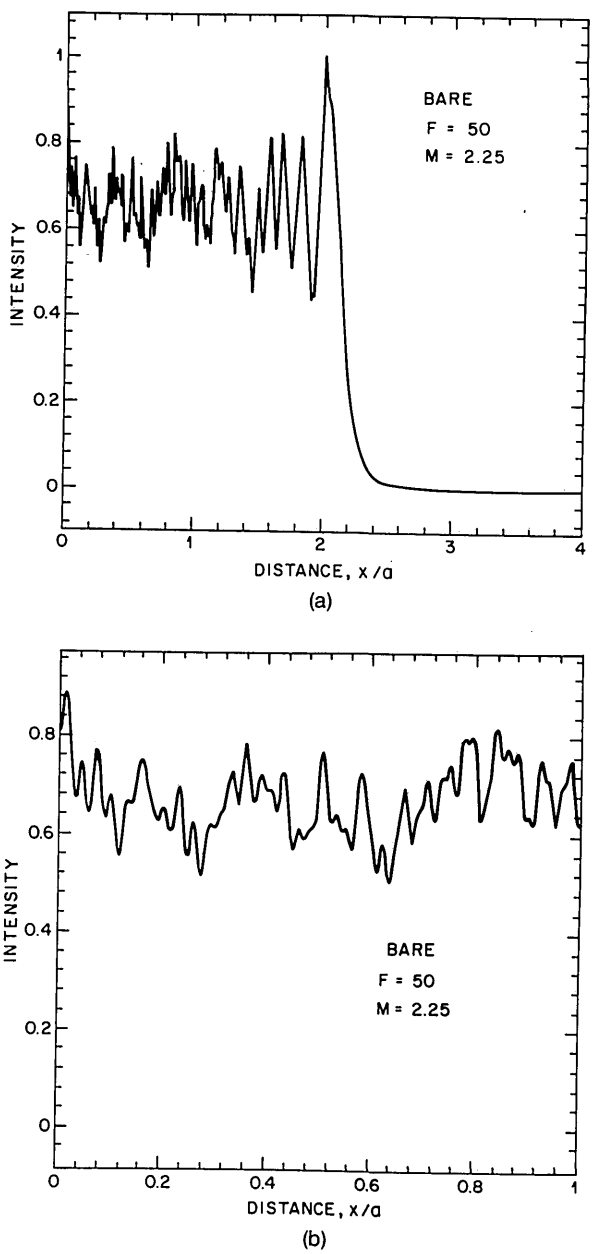

Fig. 3. Normalized intensity profile of a strip bare confocal unstable resonator with $F = 50$. The other parameters are identical to those of Fig. 2. To resolve the rapid transverse variations, (b) shows an enlarged view covering only the small-mirror region $x \leq a$.

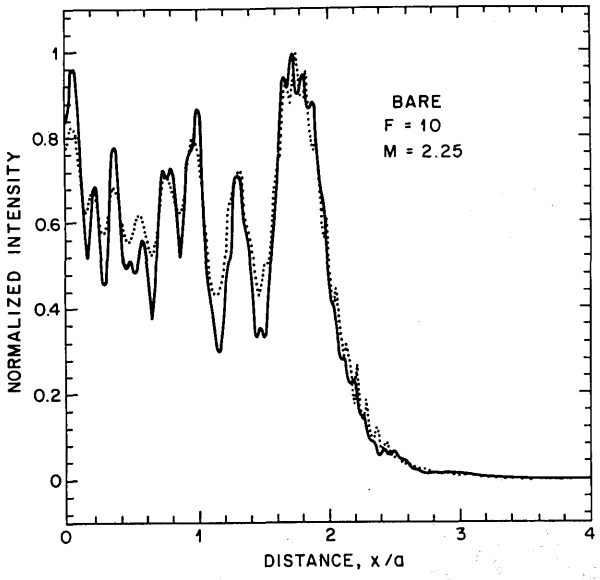

Fig. 4. Comparison of the intensity profiles obtained for a strip bare unstable resonator with $F = 10$ using CFT (solid curve) and FFT (dotted curve) algorithms.

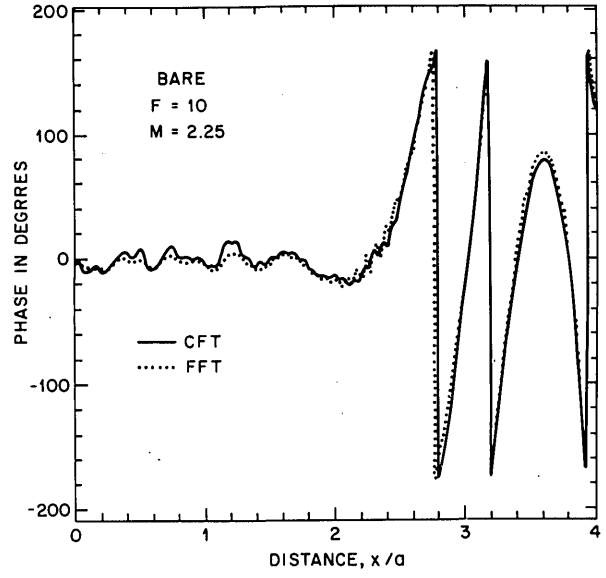

Fig. 5. Comparison of the phase profiles obtained for a strip bare unstable resonator with $F = 10$ using CFT and FFT algorithms. The rapid oscillations in phase beyond $x = Ma$ merely reflect the fact that the phase is plotted modulo 2π.

Furthermore, the use of the FFT appears to smooth out the intensity and phase profiles. Physically, this smoothing is due to a basic limitation of the FFT procedure that cannot adequately represent the sharp discontinuity at the mirror edge. By contrast, the CFT was developed to handle this discontinuity in an exact manner.[34,35] The FFT accuracy can be improved by increasing N. This was verified for a twofold increase in N to 400. For this case, the CFT results were almost unchanged, while the FFT results showed a better agreement with those of the CFT.

The case of a three-dimensional bare resonator with square mirrors is considered by choosing $N = N_x = N_y$ to be the same in the two transverse directions. The resulting intensity profile $|\psi_L(x, y, 0)|^2$ for a given y is identical, within a constant multiplicative factor, to that obtained for a strip resonator. This is not surprising, owing to linearity of Eqs. (2.8) and (2.9) in the absence of gain.

B. Loaded Resonator

For a loaded resonator the forward and backward waves experience intensity-dependent gain and phase shift during propagation inside the gain medium. These are calculated using Eq. (2.10) or (2.12) for given values of the small-signal gain g_0 and the detuning parameter Ω. We now study the effect of saturated gain on the mode profile of a loaded unstable resonator. The resonator parameters are identical to those used for the bare-resonator case. A moderately large Fresnel number $F = 10$ is chosen with $M = 2.25$, such that the

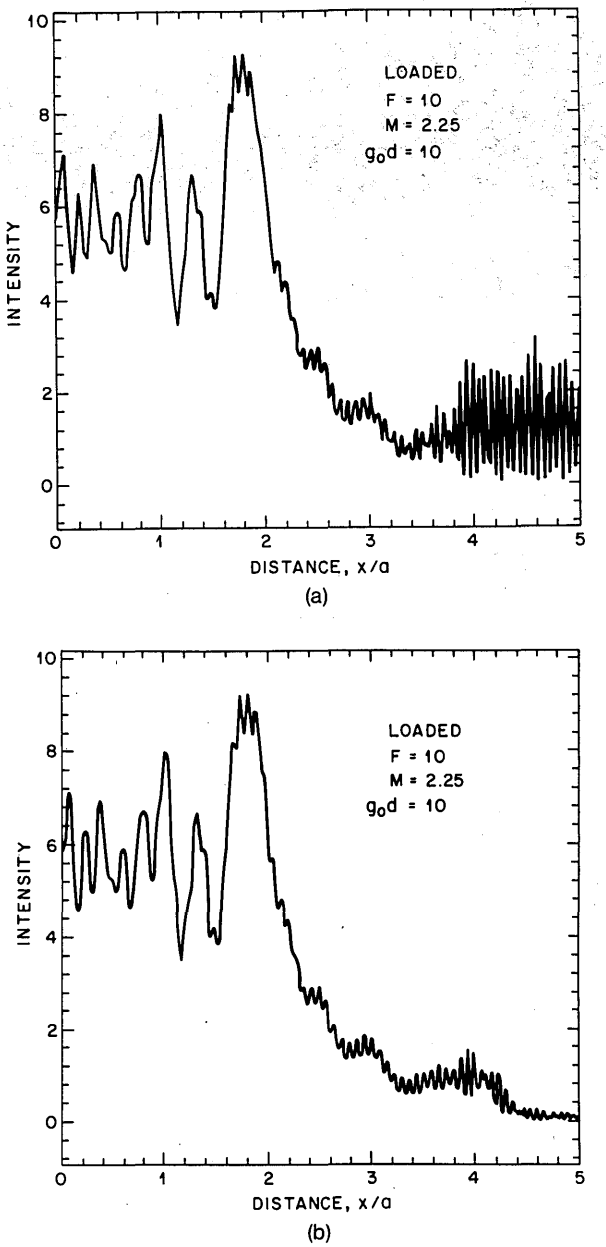

Fig. 6. Illustrating numerical instability in a loaded unstable resonator arising from the amplification of wing fluctuations. The intensity profile is shown (a) with uniform small-signal gain and (b) with the Fermi profile using Eq. (4.3) with $x_0 = 4a$. In both cases $g_0 d = 10$ and the intensity is normalized to the saturation intensity.

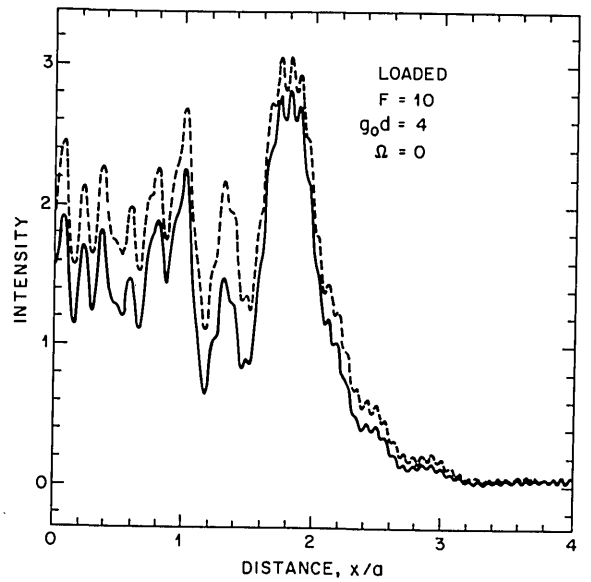

Fig. 7. Intensity profiles in a loaded unstable resonator with (solid curve) and without (dashed curve) inclusion of the standing-wave effects. The gain formulas, Eqs. (2.10) and (2.12), respectively, are used.

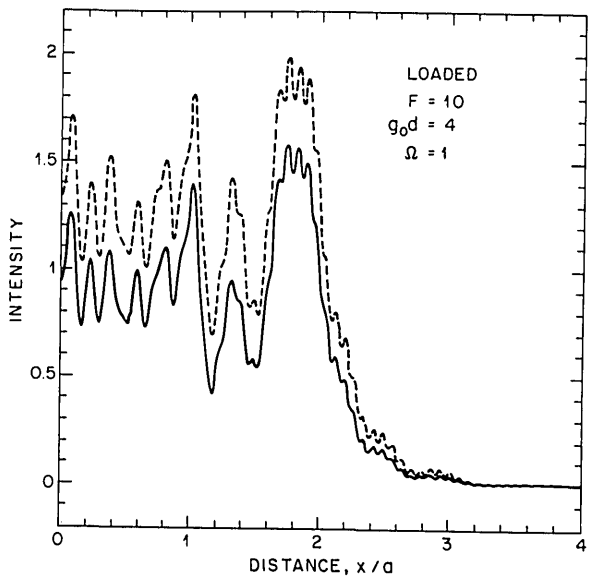

Fig. 8. Same as in Fig. 7 except that the off-resonance case is considered. Note that the standing-wave effects are more pronounced.

tube Fresnel number $F_T = M^2F \approx 50$. We consider a strip resonator with 400 mesh points and a guard-band ratio of 5. To begin with, we focus our attention on the on-resonance case and take $\Omega = 0$. In the following discussion the mode intensity is normalized to the saturation intensity $|E_s|^2$ [see Eq. (2.3)].

It should be noted that the transverse variations of small-signal gain g_0 can be readily incorporated in the computer code. If g_0 is assumed to be uniform, a problem arises since small fluctuations in the wings of the mode profile are significantly amplified during each round trip. This could lead to numerical instability for the high-gain case, as shown in Fig. 6 for $g_0d = 10$. As we mentioned in Section 4, the instability can be avoided by using a gain cut so that g_0 reduces to zero in the wings of the mode profile [see Eq. (4.3)]. This is not a limitation since real devices have a gain medium of fine extent. Figure 6(b) shows the effect of using the Fermi-function gain profile given by Eq. (4.3). As is evident, amplified wing fluctuations are suppressed, while the mode structure remains unaffected.

As we mentioned in Section 2, interference between the forward and backward waves in a standing-wave cavity modifies the gain experienced by them. This is a new feature not included in previous work.[18–24] The modified gain formula (2.10) was used in Ref. 27 to study interference effects in an unstable resonator in the geometrical-optics approximation ($F = \infty$). Figure 7 shows the change in the mode profile that is due to standing-wave interference for $F = 10$ and $g_0d = 4$. Although the qualitative features remain unchanged, significant quantitative deviations (up to 30%) occur. It is interesting to note that the detailed mode structure is largely unaffected, i.e., the number of peaks and their relative positions remain the same. This can be understood by noting that peak positions are governed by edge diffraction and the gain only enhances the amplitude of each peak. The effect of standing-wave interference is to reduce the peak heights. Clearly, the extracted power would also be less.[42]

To see the effect of saturated gain on the mode profile, Fig. 7 should be compared with Fig. 4 obtained for a bare resonator with the same value of F. Again, we note that the features such as the number of peaks and their relative positions are unaffected by gain, supporting the view that they represent a manifestation of edge diffraction.[31] However, each peak is amplified by a different amount, and the overall intensity distribution changes significantly with gain. A qualitatively similar behavior is found to occur for three-dimensional loaded unstable resonators.

Finally, we consider the off-resonance case when the laser is detuned from the gain-line center. Figure 8 shows the intensity distribution for $\Omega = 1$, corresponding to the shift of the laser frequency by an amount equal to the homogeneous line width. The other parameters are identical to those in Fig. 7. The mode profiles are shown with and without including the standing-wave interference effects. A direct comparison of Figs. 7 and 8 shows that the laser detuning from the gain-line center reduces the power carried by the mode without affecting the detailed mode structure. Further, the standing-wave effects are now more pronounced. These results are in qualitative agreement with and support those obtained previously[27] in the geometrical-optics approximation.

6. CONCLUSIONS

The electromagnetic-field distribution in loaded unstable resonators is considered using an iterative approach based on the beam-propagation method. By a simultaneous integration of the forward and backward waves, storage requirements are minimized so that the resulting code can be used for large Fresnel numbers. To account for edge diffraction occurring at the small mirror, a CFT algorithm is developed and used. We find that the use of FFT invariably produces smoothing of the mode profile unless an extraordinarily large number of mesh points are used. For our calculations we have used a modified gain formula that incorporates the effects of interference between the forward and backward waves. It is found that this interference reduces the mode power significantly,

and the relative decrease increases with the detuning of the laser frequency from the gain-line center. Since the interference effects become less important for a flowing gain medium, the axial gas flow may help to increase the power extraction efficiency of a high-power laser system. An important result is that the saturated gain does not alter the number of peaks and their relative positions in the near-field intensity distribution. This supports the view that these features arise from edge diffraction[31] and the saturated gain simply amplifies each peak, albeit by a different amount depending on the peak intensities.

APPENDIX A: OUTLINE OF THE CONTINUOUS-FOURIER-TRANSFORM ALGORITHM

The CFT algorithm used here is based on a quadrature formula for Fourier integrals derived by Marsden and Taylor[47] in which the integral

$$g(\mu) = \int_a^b \exp(i\mu x) f(x)\mathrm{d}x \tag{A1}$$

is approximated by

$$g(\mu) = hAB\left[\sum_{j=0}^{N} \exp(i\mu x_j) f(x_j) - \tfrac{1}{2}f(x_0)e^{i\mu a} - \tfrac{1}{2}f(x_N)e^{i\mu b}\right] - ihA \times \sum_{r=0}^{k-1} i^r h^r C_r [f^{(r)}(x_N)e^{i\mu b} - f^{(r)}(x_0)e^{i\mu a}] + Rf, \tag{A2}$$

where $h = (b-a)/N$ and $x_j = a + hj$. The coefficients $A(\mu h, k)$, $B(\mu h, k)$, and $C_r(\mu h, k)$ are chosen so that the error Rf vanishes when $f(x)$ is a spline of order k with knots at x_j for k even and at $x_j + \frac{1}{2}h$ for k odd. For $k = 4$ (a cubic spline) and $u = \mu h$, these coefficients are given by[47]

$$A = 3/(2 + \cos u), \tag{A3}$$

$$B = [(2/u)\sin(u/2)]^4, \tag{A4}$$

$$C_0 = [u^3(2 + \cos u) - 12\sin^2(u/2)\sin u]/3u^4, \tag{A5a}$$

$$C_1 = [u^2(2 + \cos u) - 12\sin^2(u/2)]/3u^4, \tag{A5b}$$

$$C_2 = [u(2 + \cos u) - 3\sin(u/2)]/3u^4, \tag{A5c}$$

$$C_3 = 0. \tag{A5d}$$

For small u expressions (A4) and (A5) for B and C_r are numerically unstable and must be replaced by a power series in u. Such power series were given by Einarsson[48] for the cubic spline. However, the quadrature formula (A2) of Marsden and Taylor[47] is completely general and holds for all k.

Equation (A2) is directly applicable when the function $f(x)$ is known. In our application to field propagation in unstable resonator cavities, however, $f(x)$ is known only at the mesh points x_j, and the function derivatives $f^{(r)}(x)$ required in Eq. (A2) are not readily available. Instead, we have used a third-order forward (backward) difference approximation to the function derivatives at the left (right) end points, respectively. Marsden and Taylor,[47] citing a theorem of Swartz and Varga,[49] have pointed out that this approximation should result in formulas for which the optimal error still obtains.

Since in many applications the transform $g(\mu)$ is required for generally many values of μ, a numerically efficient evaluation of the first summation in Eq. (A2) is desirable. We consider a uniformly spaced set of frequencies:

$$\mu = \mu_0 + m\Delta\mu, \qquad m = 0, 1, \ldots M. \tag{A6}$$

For $M = N$, $\mu_0 = 0$, and $\Delta\mu = 2\pi/(b-a)$, this summation may be carried out directly by using the FFT. However, for many applications this choice is unnecessarily restrictive. For arbitrary M, μ_0, and $\Delta\mu$, the sum

$$s_m = \sum_{j=0}^{N-1} \exp[i(\mu_0 + \Delta\mu m)hj] f_j \tag{A7}$$

may be evaluated by using the remarkable chirp z transform,[46] which, for a given input sequence ψ_n obtains

$$\phi_m = \sum_{n=0}^{N-1} z_m{}^{-n}\psi_n, \qquad m = 0, 1, \ldots, M-1, \tag{A8}$$

with z given quite generally by

$$z_m = z_0 W^{-m}, \tag{A9}$$

and in a time proportional to $L \log_2 L$, where L is the number of points in the FFT used internally by the chirp z transform and must satisfy

$$L \geq M + N - 1. \tag{A10}$$

Comparison of Eqs. (A6) and (A7) with Eqs. (A8) and (A9) suggests the assignments

$$z_0 = \exp[-i\mu_0 h], \qquad W = \exp[i\Delta\mu h] \tag{A11}$$

for the evaluation of Eq. (A7).

ACKNOWLEDGMENTS

This research at the City College of New York was supported in part by a grant from the U.S. Department of Energy, Office of Basic Energy Sciences; the Division of Material Sciences, U.S. Army Research Office; and the City University of New York PSC-CUNY Research Award Program.

M. Lax is also with AT&T Bell Laboratories, Murray Hill, New Jersey 07974.

* Present address, Institute for Physics, P.O.B. 57 11001, Beograd, Yugoslavia.

† Present address, Philips Laboratories, Briarcliff Manor, New York 10510.

‡ Deceased.

REFERENCES

1. A. E. Siegman, "Unstable optical resonators," Appl. Opt. **13**, 353–367 (1974); we refer to this paper for a review and for an extensive bibliography of the work on unstable resonators before 1974.
2. D. B. Rensch and A. N. Chester, "Iterative diffraction calculations of transverse mode distributions in confocal unstable laser resonators," Appl. Opt. **12**, 997–1010 (1973).
3. T. F. Ewanizky and J. M. Craig, "Negative-branch unstable resonator Nd:YAG laser," Appl. Opt. **15**, 1465–1469 (1976).
4. R. Chodzko, S. B. Mason, and E. F. Cross, "Annular converging wave cavity," Appl. Opt. **15**, 2137–2144 (1976).
5. A. A. Isaev, M. A. Kazaryan, G. G. Petrash, S. G. Rautian, and A. M. Shalagin, "Shaping of the output beam in a pulsed gas laser

with an unstable resonator," Sov. J. Quantum Electron. **7**, 746–752 (1977).
6. P. B. Mumola, H. J. Robertson, G. N. Steinberg, J. L. Kreuzer, and A. W. McCullough, "Unstable resonator for annular gain volume lasers," Appl. Opt. **17**, 936–943 (1978).
7. P. W. Milonni and A. H. Paxton, "Model for the unstable resonator carbon monoxide electric-discharge laser," J. Appl. Phys. **42**, 1012–1026 (1978).
8. R. J. Dewhurst and D. Jacoby, "A mode-locked unstable Nd:YAG laser," Opt. Commun. **28**, 107–110 (1979).
9. W. H. Steier, "Unstable Resonators," in *Laser Handbook*, M. L. Stitch, ed. (North-Holland, Amsterdam, 1979), Vol 3, pp. 3–39.
10. P. Horwitz, "Asymptotic theory of unstable resonator modes," J. Opt. Soc. Am. **63**, 1528–1543 (1973).
11. R. R. Butts and P. V. Avizonis, "Asymptotic analysis of unstable laser resonators with circular mirrors," J. Opt. Soc. Am. **68**, 1072–1078 (1978).
12. L. W. Chen and L. B. Felson, "Coupled-mode-theory of unstable resonators," IEEE J. Quantum Electron. **QE-9**, 1102–1113 (1973).
13. I. M. Bel'dyugin, E. M. Zemskov, A. Kh. Mamyan, and V. N. Seminogov, "Theory of open resonators with cylindrical mirrors," Sov. J. Quantum Electron. **4**, 484–490 (1974).
14. A. A. Isaev, M. A. Kazaryan, G. G. Petrash, and S. G. Rautian, "Converging beams in unstable telescopic resonators," Sov. J. Quantum Electron. **4**, 761–766 (1974).
15. C. Santana and L. B. Felson, "Unstable open resonators: two-dimensional and three-dimensional losses by a waveguide analysis," Appl. Opt. **15**, 1470–1478 (1976).
16. S. H. Cho, S. Y. Shin, and L. B. Felson, "Ray-optical analysis of cylindrical unstable resonators," J. Opt. Soc. Am. **69**, 563–574 (1979).
17. S. H. Cho and L. B. Felson, "Ray-optical analysis of unstable resonators with spherical mirrors," J. Opt. Soc. Am. **69**, 1377–1384 (1979).
18. A. E. Siegman and E. A. Sziklas, "Mode calculation in unstable resonators with flowing saturable gain. I: Hermite–Gaussian expansion," Appl. Opt. **13**, 2775–2792 (1974).
19. E. A. Sziklas and A. E. Siegman, "Mode calculation in unstable resonators with flowing saturable gain. II: Fast Fourier transform method," Appl. Opt. **14**, 1874–1889 (1975).
20. Yu. A. Anan'ev, L. V. Koval'chuk, V. P. Trusov, and V. E. Sherstobitov, "Method for calculating the efficiency of lasers with unstable resonators," Sov. J. Quantum Electron. **4**, 659–664 (1974).
21. Yu. N. Karamzin and Yu. B. Konev, "Numerical investigation of the operation of unstable telescopic resonators allowing for diffraction and saturation in the active medium," Sov. J. Quantum Electron. **5**, 144–148 (1975).
22. V. S. Rogov and M. M. Rikenglaz, "Numerical investigation of the influence of optical inhomogeneities of the active medium on the operation of an unstable telescopic resonator," Sov. J. Quantum Electron. **7**, 18–21 (1977).
23. C. Santana and L. B. Felson, "Effects of medium and gain inhomogeneities in unstable optical resonators," Appl. Opt. **16**, 1058–1066 (1977).
24. G. T. Moore and R. J. McCarthy, "Theory of modes in a loaded strip confocal unstable resonator," J. Opt. Soc. Am. **67**, 228–241 (1977).
25. W. H. Louisell, M. Lax, G. P. Agrawal, and H. W. Gatzke, "Simultaneous forward and backward integration for standing waves in a resonator," Appl. Opt. **18**, 2730–2731 (1979).
26. M. Lax, G. P. Agrawal, and W. H. Louisell, "Continuous Fourier-transform spline solution of unstable resonator field distribution," Opt. Lett. **9**, 303–305 (1979).
27. G. P. Agrawal and M. Lax, "Effects of interference on gain saturation in laser resonators," J. Opt. Soc. Am. **69**, 1717–1719 (1979).
28. M. J. Smith, "Mode properties of strip confocal unstable resonators with saturable gain," Appl. Opt. **20**, 1611–1620 (1981).
29. K. E. Oughstun, "Intracavity adaptive optic compensation of phase aberrations. I: Analysis," J. Opt. Soc. Am. **71**, 862–872 (1981); Part II, J. Opt. Soc. Am. **71**, 1180–1192 (1981).
30. W. P. Latham, Jr., and M. E. Smithers, "Diffractive effect of a scraper in an unstable resonator," J. Opt. Soc. Am. **72**, 1321–1327 (1982).
31. K. E. Oughstun, "Intracavity adaptive optic compensation of phase aberrations. III: Passive and active cavity study for a large N_{eq} resonator," J. Opt. Soc. Am. **73**, 282–302 (1983).
32. M. E. Smithers and T. R. Ferguson, "Unstable optical resonators with linear magnification," Appl. Opt. **23**, 3718–3724 (1984).
33. P. W. Milonni, "Criteria for the thin-sheet gain approximation," Appl. Opt. **16**, 2794–2795 (1977).
34. M. Lax and G. P. Agrawal, "Evaluation of Fourier integrals using *B*-splines," Math. Comput. **39**, 535–548 (1982).
35. B. Coffey and M. Lax, "Two efficient continuous Fourier transform algorithms for unstable resonator simulation," Appl. Opt. (to be published).
36. M. Sargent III, M. O. Scully, and W. E. Lamb, Jr., *Laser Physics* (Addison-Wesley, Reading, Mass., 1974), Chap. 8.
37. M. Lax, W. H. Louisell, and W. B. McKnight, "From Maxwell to paraxial wave optics," Phys. Rev. A **11**, 1365–1370 (1975).
38. D. O. Riska and S. Stenholm, "The influence of the mode structure on the quantum theory of the laser," Phys. Lett. **30A**, 16–17 (1969).
39. H. J. Carmichael, "The mean-field approximation and validity of a truncated Bloch hierarchy in an absorptive bistability," Opt. Acta **27**, 147–158 (1980).
40. G. P. Agrawal and H. J. Carmichael, "Inhomogeneous broadening and the mean-field approximation for optical bistability in a Fabry–Perot," Opt. Acta **27**, 651–660 (1980).
41. H. J. Carmichael and J. A. Hermann, "Analytic description of optical bistability including spatial effects," Z. Phys. B **38**, 365–380 (1980).
42. G. P. Agrawal and M. Lax, "Analytic evaluation of interference effects on laser output in a Fabry–Perot resonator," J. Opt. Soc. Am. **71**, 515–519 (1981).
43. J. A. Fleck, Jr., J. R. Morris, and M. D. Feit, "Time-dependent propagation of high energy laser beams through the atmosphere," Appl. Phys. **10**, 129–160 (1976), App. A.
44. M. Lax, J. H. Batteh, and G. P. Agrawal, "Channeling of intense electromagnetic beams," J. Appl. Phys. **52**, 109–125 (1981).
45. J. W. Cooley and J. W. Tukey, "An algorithm for the machine calculation of complex Fourier series," Math. Comput. **19**, 297–301 (1965).
46. L. R. Rabiner and C. M. Radar, eds., *Digital Signal Processing* (Institute of Electrical and Electronics Engineers, New York, 1972).
47. M. J. Marsden and G. D. Taylor, "Numerical evaluation of Fourier integrals," in *Numerische Methoden der Approximations Theorie* (Birkhauser, Basel, 1972), Band 16, pp. 61–76.
48. B. Einarsson, "Numerical calculation of Fourier integrals with cubic splines," Nord. Tidsskr. Informationsbehand. **8**, 279–286 (1968).
49. B. K. Swartz and R. S. Varga, "Error bounds for spline and *L*-spline interpolations," J. Approx. Theory **6**, 6–49 (1972).